

# Self-accelerating solitons

Boris A. Malomed<sup>1,2</sup>

<sup>1</sup>*Department of Physical Electronics, School of Electrical Engineering, Faculty of Engineering, and Center for Light-Matter Interaction, Tel Aviv University, Tel Aviv 69978, Israel*

<sup>2</sup>*Instituto de Alta Investigación, Universidad de Tarapacá, Casilla 7D, Arica, Chile*

Basic models which give rise to one- and two-dimensional (1D and 2D) solitons, such as the Gross-Pitaevskii (GP) equations for BEC, feature the Galilean invariance, which makes it possible to generate families of moving solitons from quiescent ones. A challenging problem is to find models admitting stable self-accelerating (SA) motion of solitons. SA modes are known in linear systems in the form of Airy waves, but they are poorly localized states. This brief review presents two-component BEC models which make it possible to predict SA solitons. In one system, a pair of interacting 1D solitons with opposite signs of the effective mass is created in a binary BEC trapped in an optical-lattice potential. In that case, opposite interaction forces, acting on the solitons with positive and negative masses, produce equal accelerations, while the total momentum is conserved. The second model is based on a system of GP equations for two atomic components, which are resonantly coupled by a microwave field. The latter model produces an exact transformation to an accelerating reference frame, thus predicting 1D and 2D stable SA solitons, including vortex rings.

**Introduction.** – A basic property of one- and two-dimensional (1D and 2D) equations which produce solitons is the Galilean invariance, which generates solitons moving with an arbitrary velocity from a quiescent one. A challenging issue is to construct localized states moving at a constant acceleration, rather than constant velocity [1, 2]. A well-known fact is that the linear Schrödinger equation,  $iu_z + (1/2)u_{xx} = 0$  (it is written in the form of the paraxial propagation equation in optics, with propagation distance  $z$  and transverse coordinate  $x$ ) admits self-accelerating (SA) solutions in the form of Airy waves [3]. Later, it was predicted [4] and experimentally demonstrated, originally in optics [5], and then in electron beams [6], plasmonics [7], Bose-Einstein condensates (BECs) [8], acoustics [9], gas discharge [10], and water waves [11] that truncated Airy waves (TAWs) can be created in these media, the respective exact solution of the linear Schrödinger equation being

$$u_{\text{TAW}}(x, z) = u_0 \text{Ai} \left( \alpha x - \frac{\alpha^4}{4} z^2 + i\aleph \alpha^2 z \right) \exp(\aleph \alpha x) \times \exp \left( -\frac{i\alpha^6}{12} z^3 + \frac{i\alpha^3}{2} xz - \frac{\aleph \alpha^4}{2} z^2 + \frac{i\aleph^2 \alpha^2}{2} z \right), \quad (1)$$

where Ai is the Airy function, and constants  $u_0$ ,  $\alpha$ , and  $\aleph > 0$  define, respectively, the amplitude, internal scale, and truncation of the Airy wave. Accordingly, the input which generates solution (1) is  $u(x; z=0) = u_0 \text{Ai}(\alpha x) \exp(\aleph \alpha x)$ . The truncation factor is necessary to make the total norm (power, in terms of optics) of the input finite:

$$N_{\text{TAW}} \equiv \int_{-\infty}^{+\infty} |u(x)|^2 dx = u_0^2 \left( \sqrt{8\pi\aleph\alpha} \right)^{-1} \exp(2\aleph^3/3), \quad (2)$$

while the TAW's momentum,

$$P = i \int_{-\infty}^{+\infty} u_x^* u dx, \quad (3)$$

is zero, in spite of the self-acceleration featured by this wave (both  $N$  and  $P$  are dynamical invariants of the Schrödinger equation).

In fact, the truncation leads to gradual degradation of the TAW, as shown, in particular, by factor  $\exp(-\aleph \alpha^4 z^2/2)$  in solution (1). Another source of degradation is the action of nonlinearity, as TAW is the eigenmode of the linear medium. Effects of nonlinearity on the Airy waves were considered in many works [12]–[18], chiefly demonstrating decay into solitons.

A possibility to create well-localized (unlike the Airy waves) SA two-component pulses in optics was elaborated in terms of a system of coupled nonlinear Schrödinger (NLS) equations with opposite signs of the group-velocity dispersion (GVD) in them [19], aiming to create two pulse components with *opposite signs of their effective masses*. In this case, the opposite interaction forces with which the coupled components act on each other give rise to identical signs of the acceleration. A solution for such an SA bound state was constructed approximately, taking an unperturbed NLS soliton in the anomalous-GVD component, and applying the Thomas-Fermi approximation to the normal-GVD

one. The so predicted optical SA pulses were demonstrated experimentally in a roughly similar temporal-domain form, using a pair of fiber loops with different lengths, coupled to each other at one point [20].

It is relevant to mention that a soliton moving with a constant acceleration (although not of the SA type) can be readily predicted taking the single NLS equation with the self-attractive cubic term and an attractive or repulsive local defect which moves with acceleration  $a$ :

$$iu_z + (1/2)u_{xx} + |u|^2u = -\varepsilon\delta(x - az^2/2)u, \quad (4)$$

where  $\delta$  is the delta-function,  $\varepsilon > 0$  or  $\varepsilon < 0$  corresponding to the attractive or repulsive defect, respectively. In terms of the spatial-domain NLS equation (4) in optics, the “accelerating” defect represents a narrow parabolic ( $x = az^2/2$ ) stripe in the  $(x, z)$  plane, with the locally increased ( $\varepsilon > 0$ ) or decreased ( $\varepsilon < 0$ ) value of the refractive index. It is convenient to rewrite Eq. (4) in the co-moving reference frame, applying the corresponding boost transformation [1]:

$$\xi \equiv x - az^2/2, u(x, z) \equiv v(\xi, z) \exp(ia\xi z + ia^2z^3/6), \quad (5)$$

$$iv_z + (1/2)v_{\xi\xi} + |v|^2v = a\xi v - \varepsilon\delta(\xi)v. \quad (6)$$

In the moving frame, the soliton may be approximated by the simple stationary solution to Eq. (6),

$$v_{\text{sol}}(\xi, z) = (N/2)\text{sech}((N/2)(\xi - \xi_0)) \exp(iN^2z/8), \quad (7)$$

where  $N$  is the soliton’s norm (see Eq. (2)), and  $\xi_0$  is a shift of the soliton from the position of the defect. Treating the terms on the right-hand side of Eq. (6) by perturbations [21], the soliton is considered as a quasi-particle under the action of an effective potential,

$$U(\xi_0) = Na\xi_0 - (\varepsilon N^2/4) \text{sech}^2(N\xi_0/2). \quad (8)$$

This potential has an equilibrium position with sign  $\text{sgn}(\xi_0) = -\text{sgn}(a\varepsilon)$ , which exists, for given strength  $\varepsilon$  of the defect, if the acceleration does not exceed a critical value,

$$|a_{\text{max}}| = |\varepsilon|N^2/(6\sqrt{3}). \quad (9)$$

The corresponding largest equilibrium value of the shift is  $(|\xi_0|)_{\text{max}} = N^{-1} \ln((\sqrt{3} + 1)^2/2) \approx 1.32/N$ . Note that the largest acceleration with which the soliton can be dragged by the moving defect, as given by Eq. (9), does not depend on the sign of  $\varepsilon$ .

A different result is produced for dragging solitons by the local defect moving with constant acceleration in the framework of the NLS equation with the quintic, rather than cubic, nonlinearity (which may also be realized in optical media [22]),

$$iu_z + (1/2)u_{xx} + |u|^4u = -\varepsilon\delta(x - az^2/2)u. \quad (10)$$

In the uniform space ( $\varepsilon = 0$ ), Eq. (10) gives rise to commonly known *1D Townes solitons* [23],  $u = (3k)^{1/4} \sqrt{\text{sech}(2\sqrt{2k}x)} \exp(ikz)$ , with arbitrary propagation constant  $k > 0$ . This soliton family is degenerate,

as its norm takes a single value, which does not depend on  $k$ ,  $N = \sqrt{3/2}\pi/2$ , and the family is completely unstable against the onset of the critical collapse [24]. However, all the solitons are *stabilized* by the interaction with the quiescent attractive defect ( $a = 0, \varepsilon > 0$ ) [25]. Then, the above consideration can be developed for the solitons of Eq. (10) pulled by the defect with constant acceleration. In particular, the largest acceleration which can be supported by the defect with given  $\varepsilon > 0$  is  $|a_{\text{max}}| = (4/\pi)\varepsilon k$ , cf. Eq. (9).

The objective of this *perspective* is to produce a brief summary of results which predict possibilities of true SA motion of 1D and 2D solitons in specific BEC models, one based on the spatially-periodic optical-lattice (OL) potential, and another one making use of a binary BEC whose components are resonantly coupled by a microwave (MW) field.

**Co-accelerating bound states of solitons with positive and negative masses.** – A two-component model which allows one to predict stable SA bound states of solitons with positive and negative effective masses is represented by a system of Gross-Pitaevskii (GP) equations for wave functions  $\phi$  and  $\psi$  of the binary BEC, including the spatially-periodic potential of the OL type in each equation, with strengths  $U_1$  and  $U_2$  [26]:

$$\begin{aligned} i\phi_t &= -(1/2)\phi_{xx} - [g_1|\phi|^2 + \gamma|\psi|^2 + U_1 \cos(2\pi x) + fx] \phi, \\ i\psi_t &= -(1/2)\psi_{xx} - [\gamma|\phi|^2 - g_2|\psi|^2 + U_2 \cos(2\pi x) + fx] \psi. \end{aligned} \quad (11)$$

Here,  $g_1 > 0$  and  $-g_2 < 0$  are coefficients of the self-interaction of the components, implying that their signs are made opposite by means of the Feshbach resonance applied to one of the components [27], and  $\gamma > 0$  is the coefficient of the cross-attraction. The OL period in Eq. (11) is set equal to 1 by means of rescaling. The system also includes a possibility to consider the action of gravity, with strength  $f$ , on both components.

*Analytical considerations.* To provide opposite signs of the effective mass for solitons in components  $\phi$  and  $\psi$ , it is natural to consider the case when quasi-wavenumbers of wave functions  $\phi$  and  $\psi$  are set to be close, respectively, to the center and edge of the first OL's Brillouin zone. The respective effective masses, calculated by means of the known methods for the linear GP equation [28–30], are, respectively,

$$M_1 = \frac{2\pi^3 + U_1^2 + \pi^2 \sqrt{4\pi^4 + 2U_1^2}}{10\pi^4 + U_1^2 - 3\pi^2 \sqrt{4\pi^4 + 2U_1^2}}, \quad (12)$$

$$-M_2 = U_2 / (U_2 - 2\pi^2) \quad (13)$$

( $M_2$  is defined with sign minus, to focus on the relevant case of the negative mass, which means  $M_2 > 0$ ), and the wave functions themselves are approximated by

$$\phi(x) = \Phi(x) \frac{1 + 2a \cos(2\pi x)}{\sqrt{1 + 2a^2}}, \psi(x) = \sqrt{2} \Psi(x) \cos(\pi x), \quad (14)$$

with  $a \equiv \sqrt{(\pi^2/U_1)^2 + 1/2 - \pi^2/U_1}$ , where  $\Phi(x)$  and  $\Psi(x)$  are slowly varying (in comparison with  $\cos(2\pi x)$ ) envelopes. Actually, the negative mass is a characteristic feature of gap solitons, generated by the interplay of the OL potential and self-repulsion [29].

The substitution of expressions (14) in Eqs. (11) leads, by means of the averaging procedure, to equations governing the slow evolution of the envelope amplitudes, which do not include the OL potential,

$$i \frac{\partial \Phi}{\partial t} = -\frac{1}{2M_1} \frac{\partial^2 \Phi}{\partial x^2} - (G_1 |\Phi|^2 + \Gamma |\Psi|^2 + fx) \Phi, \quad (15)$$

$$i \frac{\partial \Psi}{\partial t} = \frac{1}{2M_2} \frac{\partial^2 \Psi}{\partial x^2} - (\Gamma |\Phi|^2 - G_2 |\Psi|^2 + fx) \Psi, \quad (16)$$

with effective nonlinearity coefficients,

$$G_1 = g_1 \frac{1 + 12a^2 + 6a^4}{(1 + 2a^2)^2}, G_2 = \frac{3}{2} g_2, \\ \Gamma = \frac{1 + 2a^2 + 2a}{1 + 2a^2} > 0. \quad (17)$$

Sign minus is eliminated in front of the second derivative in Eq. (16) according to the definition of the respective effective mass in Eq. (13). Note that Eqs. (15) and (16) conserve the total momentum of wave functions  $\Phi$  and  $\Psi$  (cf. Eq. (3)), in spite of the possibility to produce SA states, as shown below.

It is obvious that Eqs. (15) and (16) may indeed feature opposite signs of the effective masses, if  $M_1$  and  $M_2$  are both positive (or both negative), and opposite signs of the self-interaction in the two components, if  $G_1$  and  $G_2$  are both positive (or both negative) too. These sign combinations open the way to the creation of coupled pairs of solitons with opposite signs of their dynamical masses.

Using the Lagrangian structure of Eqs. (15) and (16), the variational approximation (VA) can be applied to the system, using the following ansatz for two-component solitons:

$$\{\Phi, \Psi\} = \sqrt{N_{1,2}} (2\alpha_{1,2}/\pi)^{1/4} \exp \left[ i\varphi_{1,2} - \alpha_{1,2} (x - \xi_{1,2})^2 + ik_{1,2} (x - \xi_{1,2}) \right], \quad (18)$$

with norms  $N_{1,2}$ , widths  $\alpha_{1,2}^{-1/2}$ , central coordinates  $\xi_{1,2}$ , momenta  $k_{1,2}$ , and phases  $\varphi_{1,2}$ . The VA procedure [31] leads to equations of motion for the coordinates in the absence of gravity ( $f = 0$ ) [26]:

$$\frac{d^2 \xi_{1,2}}{dt^2} = \frac{N_{2,1}}{M_{1,2}} \alpha \exp \left[ -\frac{2\alpha_1 \alpha_2}{\alpha_1 + \alpha_2} (\xi_1 - \xi_2)^2 \right] (\xi_2 - \xi_1), \quad (19)$$

$$\alpha \equiv (2\Gamma/\sqrt{\pi}) (2\alpha_1 \alpha_2 / (\alpha_1 + \alpha_2))^{3/2}, \rho \equiv N_2/M_1 - N_1/M_2. \quad (20)$$

Further, in the linear approximation with respect to  $\Delta\xi \equiv \xi_2 - \xi_1$  Eq. (19) gives rise to the following equations for  $\Delta\xi$  and the mean coordinate,  $\Xi \equiv (\xi_1 + \xi_2)/2$ :

$$\frac{d^2\Delta\xi}{dt^2} = -\alpha\rho\Delta\xi, \quad \frac{d^2\Xi}{dt^2} = n\Delta\xi, \quad n \equiv \frac{\alpha}{2} \left( \frac{N_2}{M_1} + \frac{N_1}{M_2} \right). \quad (21)$$

In the case of  $\rho > 0$  (see Eq. (20)), the solution of Eqs. (21) predicts shuttle motion of the bound state of the solitons with positive and negative masses, combined with its inner oscillations:

$$\Delta\xi(t) = \Delta\xi_0 \cos(\sqrt{\alpha\rho}t), \quad \Xi(t) = \frac{n}{\alpha\rho} \Delta\xi_0 [1 - \cos(\sqrt{\alpha\rho}t)], \quad (22)$$

where  $\Delta\xi_0$  is an arbitrary amplitude of the oscillations. Examples of the shuttle motion produced by numerical simulations of Eqs. (15) and (16) are displayed below in Figs. 1(b) and 2(a).

The SA motion of the two-soliton bound state is predicted at  $\rho = 0$ , i.e., as it follows from Eq. (20), for relation  $N_1/N_2 = M_2/M_1$  between the norms and effective masses of the two components. This condition provides cancellation of the force driving the evolution of  $\Delta\xi$ . In this case, Eqs. (22) demonstrate that the separation  $\Delta\xi_0$  between centers of the components remains constant, and the solitons move with identical accelerations, so that  $\Xi(t) = (n/2)\Delta\xi_0 t^2$ . Examples of the SA motion produced by simulations of Eqs. (15) and (16) are presented below in Figs. 1(a) and 2(a). Finally, in the case of  $\rho < 0$  Eqs. (21) predict the exponential growth of  $\Delta\xi(t)$ , i.e., splitting of the two-soliton pair, which is also confirmed by direct numerical solutions.

Further, the VA was extended to include the gravity terms in Eqs. (15) and (16). A straightforward analysis predicts the shift of the point at which the SA state appears from  $\rho = 0$  at  $f = 0$  to  $\rho = -(M_1 M_2 \alpha \Delta\xi)^{-1} (M_1 + M_2) \exp[2\alpha_1 \alpha_2 (\alpha_1 + \alpha_2)^{-1} (\Delta\xi)^2] f$ . Thus, the gravity may be used to control the occurrence of the SA regime. The appropriate value of  $f$  can be tuned, in turn, by varying the angle,  $\Theta$ , between the vertical axis and direction of the quasi-1D waveguide into which the BEC is loaded:  $f = f_{\max} \cos \Theta$ .

*Numerical results.* Typical examples of the dynamics of the bound states of solitons with effective positive and negative masses, produced by simulations of Eqs. (15) and (16) with parameters and inputs

$$M_1 = 1, G_1 = 0.9, \Gamma = 0.1, G_2 = 0.1 + M_2^{-1}, \quad (23)$$

$$\Phi_0 = \text{sech } x, \Psi_0 = \text{sech}(x - \Delta\xi), \Delta\xi = 0.1 \quad (24)$$

(i.e., the soliton norms are  $N_1 = N_2 = 2$ ) are displayed in Fig. 1. In particular,  $M_2^{-1} = 1$  and  $M_2^{-1} = 0.96$  in Figs. 1(a) and (b) correspond, respectively to  $\rho = 0$  and  $\rho = 0.08$  (see Eq. (20)), which, in agreement with the VA prediction, produce the SA and shuttle motion, respectively. For values of  $M_2^{-1} > 1$ , i.e.,  $\rho < 0$ , the simulations demonstrate splitting of the two-soliton state, also as predicted by the VA (not shown here).

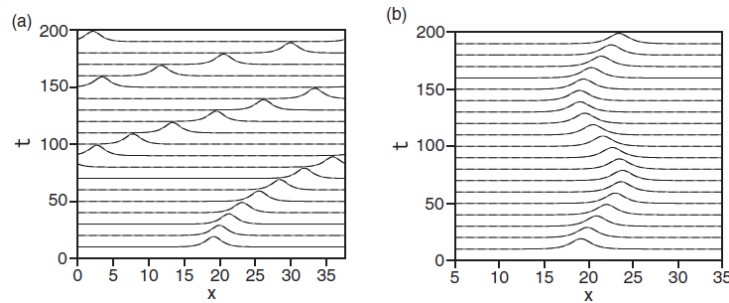


FIG. 1: The evolution of  $|\Phi(x, t)|$  and  $|\Psi(x, t)|$  (nearly overlapping solid and dashed lines, respectively) produced by simulations of Eqs. (16) and (15) with input (24) and parameters (23), where  $M_2^{-1} = 1$  (a) and  $M_2^{-1} = 0.96$  (b) (as per Ref. [26]).

Additional numerical results are presented in Fig. 2(a), which shows the law of motion of central coordinates for  $M_2^{-1} = 1, 0.98$ , and  $0.92$ , i.e.,  $\rho_{1;0.98;0.92} = 0; 0.04; 0.16$ , respectively. Note that ratio  $\sqrt{\rho_{0.92}/\rho_{0.98}} = 2$  exactly corresponds to the ratio of periods  $T_{0.98}/T_{0.92} = 2$ , in agreement with Eq. (22). Further, Fig. 2(b) compares the numerically measured acceleration of the SA pair and its VA-predicted counterpart, as given by Eq. (19). In the presence of the gravity in Eqs. (16) and (15), the direct simulations also accurately corroborate the VA predictions [26].

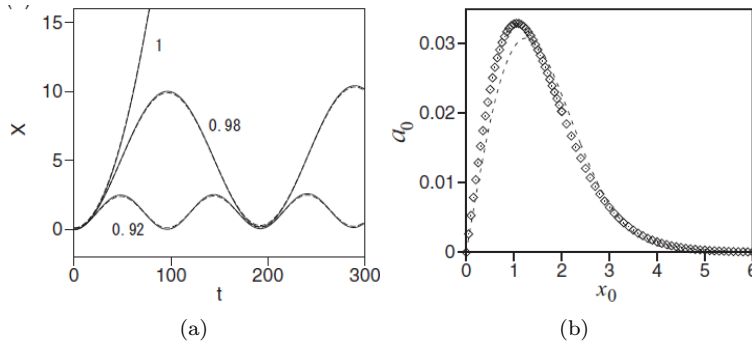


FIG. 2: (a) Trajectories of centers of the  $\Phi$  and  $\Psi$  components (solid and dashed lines, respectively), produced by the same simulations as in Fig. 1, with  $M_2^{-1} = 1, 0.92$ , and  $0.98$ , as indicated. (b) The acceleration of the SA bound state,  $a_0$ , vs. the constant separation,  $\Delta\xi \equiv x_0$ , between the bound solitons with the positive and negative masses, in the case of  $\rho = 0$  (see Eq. (20). Rhombuses: results of the simulations of Eqs. (16) and (15) with input (24) and parameters (23), where  $M_2^{-1} = 1$ . The dashed curve: the VA prediction produced by Eq. (19) (as per Ref. [26]).

The existence of robustly moving SA bound states suggest a possibility to consider collisions between such modes moving with opposite accelerations [26]. A typical example, *viz.*, collision between the same SA state which is displayed above in Figs. 1(a) and 2(a) and its mirror image is displayed in Fig. 3(a). It shows that the colliding soliton pairs pass through each other, causing increase of the separation between the bound solitons in each pair, from  $\Delta\xi = 0.10$  to  $\Delta\xi \approx 0.17$ . This, in turn, leads to the increase of the co-acceleration, in agreement with Eq. (19) and Fig. 2(b).

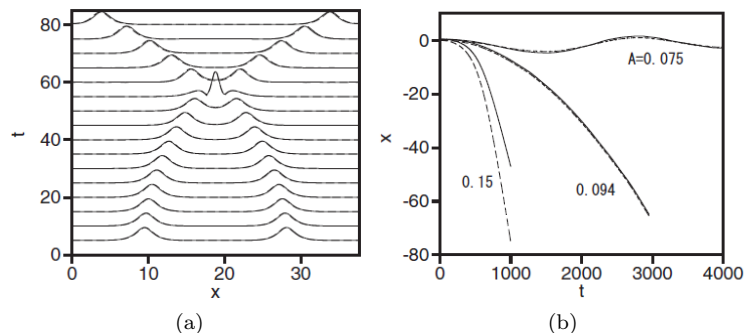


FIG. 3: (a) The collision of the SA pair, shown in Figs. 1(a) and 2(a), and its mirror image moving with the opposite self-acceleration. (b) Trajectories of motion of centers of components  $\phi$  and  $\psi$  (the continuous and dashed lines, respectively) produced by simulations of the underlying system (11), see details in the text (as per Ref. [26]).

As concerns direct simulations, the results presented above were produced by Eqs. (16) and (15), which were derived from the full system (11) as equations for the slow evolution of amplitudes  $\Phi$  and  $\Psi$  in ansatz (14). Direct simulations of the full equations produce similar results [26]. As an example, Fig. 3(b) displays trajectories of centers of the two components, as obtained from simulations of Eqs. (11) with  $U_1 = 0$ ,  $U_2 = 8$ ,  $f = 0$  (no gravity) and input given by Eq. (14), with  $\Phi(x)$  and  $\Psi(x)$  replaced by amplitudes  $A = 0.150, 0.094, 0.075$  and  $B = 0.150$ . As seen in the figure, the stable SA bound state is generated by  $A = 0.094$ , while the VA predicts, for the same input, the SA state at  $A = 0.102$ . The corresponding relative error  $\approx 0.08$  demonstrates the accuracy of the VA, in comparison with the simulations of the full underlying system (11). The shuttle motion and splitting are observed at  $A = 0.075$  and  $0.150$ , respectively, in agreement with the VA. In Ref. [32], similar simulations were performed for the system including, in addition to the OL, the quadratic potential in each component. It produces opposite forces acting on the positive- and negative-mass components, leading to their splitting.

If the solitons are considered in a more general form than defined by Eq. (14), the formation of the SA bound states of solitons with positive and negative masses is still possible (in particular, because gap solitons are mobile in the general case [29]). However, this possibility was not explored in detail.

**Self-acceleration of vortex rings (VRs) in microwave-coupled binary BEC.** – The existence of stable 2D SA solitons, including VRs, in a binary BEC formed by two atomic states  $\phi_{\uparrow,\downarrow}$ , resonantly coupled by the magnetic component  $H$  of the MW field, was predicted in Ref. [33]. The respective system of scaled GP equations for  $\phi_{\uparrow,\downarrow}$  and

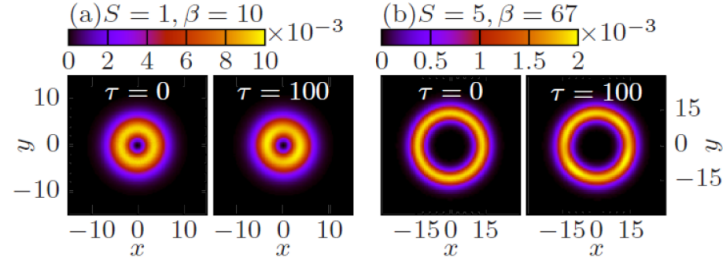


FIG. 4: Examples of the distribution of  $|\phi(r)|$  in stable VRs (vortex rings) with indicated values of  $S$  and  $\beta$ . The initial shapes of the VR ( $\tau = 0$ ) are compared to the outputs produced by simulations of Eq. (27) at time  $\tau = 100$  (as per Ref. [34]).

the Poisson equation for  $H$  are [34]

$$\begin{aligned} i \frac{\partial \phi_{\downarrow}}{\partial t} &= \left( -\frac{1}{2} \nabla^2 + \eta - \beta_c |\phi_{\uparrow}|^2 - \beta_s |\phi_{\downarrow}|^2 \right) \phi_{\downarrow} - \pi H^* \phi_{\uparrow}, \\ i \frac{\partial \phi_{\uparrow}}{\partial t} &= \left( -\frac{1}{2} \nabla^2 - \eta - \beta_c |\phi_{\downarrow}|^2 - \beta_s |\phi_{\uparrow}|^2 \right) \phi_{\uparrow} - \pi H \phi_{\downarrow}, \end{aligned} \quad (25)$$

$$\nabla^2 H = -\phi_{\downarrow}^* \phi_{\uparrow}, \quad (26)$$

where  $*$  stands for the complex conjugate,  $2\eta$  is detuning of the MW from the transition between the atomic states  $|\uparrow\rangle$  and  $|\downarrow\rangle$ ,  $\beta_c$  and  $\beta_s$  being, respectively, strengths of the cross- and self-interaction of the two components. Equations (25) are supplemented by the normalization condition,  $\int (|\phi_{\uparrow}|^2 + |\phi_{\downarrow}|^2) d\mathbf{r} = 1$ . In the symmetric system with  $\eta = 0$ , Eqs. (25) coalesce into a single one for  $\phi_{\downarrow} = \phi_{\uparrow} \equiv \phi$ , supplement by the accordingly simplified Poisson equation for real  $H$ ,

$$i \frac{\partial \phi}{\partial t} = \left[ -\frac{1}{2} \nabla^2 - \beta |\phi|^2 - \pi H \right] \phi, \quad \nabla^2 H = -|\phi|^2, \quad (27)$$

with  $\beta \equiv \beta_c + \beta_s$  and normalization  $\int |\phi(\mathbf{r})|^2 d\mathbf{r} = 1/2$ .

Numerical solutions of Eq. (27) demonstrate that it gives rise to VR solutions with chemical potential  $\mu$  and vorticity  $S = 0, 1, 2, \dots$ , in the form of  $\phi = \exp(-i\mu t + iS\theta) \Phi_S(r)$ , where  $r$  and  $\theta$  are the polar coordinates. The solutions exist in the region of  $\beta < \beta_{\max}(S)$ , where  $\beta_{\max}(S = 0) \approx 11.7$  corresponds to the commonly known value for Townes solitons [35, 36], and  $\beta_{\max}(S \geq 1)$  are the respective values for the Townes solitons with embedded vorticity [37], which are well approximated by  $\beta_{\max}(S) \approx 8\sqrt{3}\pi S$  [34]. In these intervals, the solitons with  $S = 0$  are completely stable, while the VRs are stable in narrower regions,  $\beta < \beta_{\text{st}}(S)$ . An analytical approximation yields  $\beta_{\text{st}}(S) = 2\sqrt{6}\pi S \approx 15.4S$ , while an empirical formula for the numerical results is  $\beta_{\text{st}}^{(\text{num})}(S) = 15S - 4$  [34]. Examples of stable VRs with  $S = 1$  and  $5$  are presented in Fig. 4. In intervals  $\beta_{\text{st}}(S) < \beta \leq \beta_{\max}(S)$  the VRs are unstable against splitting into necklace-shaped arrays of fragments. It is relevant to stress that the growth of  $\beta_{\text{st}}^{(\text{num})}(S) \sim S$  for the “giant” VRs (ones with large values of  $S$ ), produced by Eq. (27), makes them much more robust modes than their counterparts with smaller  $S$ . This feature is opposite to what was previously found in those models which are able to produce stable VRs with  $S > 1$  [38–45].

The finding reported in Ref. [33] is that Eqs. (27) are *exactly invariant* with respect to a boost transformation, from the quiescent reference frame to one which moves, in the 2D plane  $(x, y)$ , with vectorial acceleration  $\mathbf{a} = (a_x, a_y)$ , combined with a constant velocity,  $\mathbf{V} = (V_x, V_y)$ . The coordinates, wave functions, and magnetic field in the accelerating frame are

$$\{x', y'\} = \{x, y\} - V_{x,y}t - (a_{x,y}/2)t^2, \quad (28)$$

$$\phi'(x', y', t) = \phi(x, y, t) \exp[-i(a_x x + a_y y)t - i(V_x x + V_y y) + i\chi(t)], \quad (29)$$

$$\chi(t) = (1/6) \left[ a_x^{-1} (V_x + a_x t)^3 + a_y^{-1} (V_y + a_y t)^3 \right], \quad (30)$$

$$H'(x', y', t) = H(x, y, t) + \pi^{-1}(a_x x + a_y y). \quad (31)$$

Actually, Eqs. (28)-(31) are a generalization of the usual Galilean boost for the accelerating reference frame. Note that the solution of the 2D Poisson equation in system (27), with the source represented by a quiescent soliton, has the standard asymptotic form far from the region where the soliton is located (it is determined by the Green's function for the 2D Laplacian):

$$H(\mathbf{r}) \approx -(1/2\pi) \left( \int |\phi(\mathbf{r}')|^2 d\mathbf{r}' \right) \ln r. \quad (32)$$

The difference of the magnetic-field component (31) of the SA soliton from its quiescent counterpart (32) is the presence of the terms linear in  $x$  and  $y$ , which implies that the SA motion can be maintained by the properly constructed background magnetic field. This field provides a reservoir of the momentum which makes the self-acceleration possible.

According to Eq. (28), coordinates  $(x_c, y_c)$  of the center of the stable 2D soliton moves as  $x_c = V_x t + (1/2)a_x t^2$ ,  $y_c = V_y t + (1/2)a_y t^2$ . This is a curvilinear trajectory in the 2D plane: at small  $t$ , it is close to a straight line with slope  $x/y = V_x/V_y$ , while at  $t \rightarrow \infty$  it is close to a line with a different slope,  $x/y = a_x/a_y$ . In particular, in the case of  $a_x = V_y = 0$ , the trajectory is a parabola:

$$y_c = (a_y/2V_x^2) x_c^2. \quad (33)$$

The analytical results are corroborated by Fig. 5, which displays stably moving VRs produced by simulations of Eq. (27). The numerical solutions demonstrate exactly the same SA motion of the VRs as predicted by Eq. (33). Essentially the same results were obtained for the SA motion of solitons produced by the 1D version of Eq. (27), as

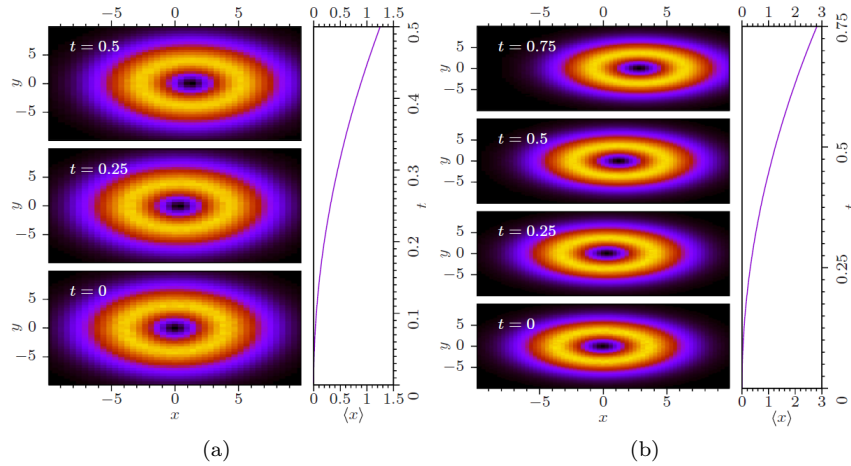


FIG. 5: (a) The plot of  $|\phi|^2$  for a self-accelerating VR with  $a_x = 10$ ,  $a_y = 0$ ,  $V_{x,y} = 0$  (see Eq. (28)), produced by the numerical solution of Eq. (27) with  $\beta = 0$ . (b) The same for  $\beta = 10$ . Right panels in (a) and (b) show the time dependence of coordinate  $\langle x \rangle$  of the VR's center, cf. Eq. (33) (as per [33]).

well as for the 2D system based on Eqs. (25) and (26) including the spin-orbit coupling between components  $\phi_\downarrow$  and  $\phi_\uparrow$  [33].

**Conclusion.** – This *perspective* represents basic models which make it possible to predict counterintuitive regimes of motion of stable 1D and 2D solitons (including vortex rings) with SA (self-acceleration). The corresponding models represent two-component BECs. In one case, a pair of interacting 1D solitons with opposite signs of the effective masses can be created in the binary BEC loaded in the OL potential [26]. In that case, the opposite interaction forces, applied to the solitons with opposite signs of the mass, produce the SA motion, similar to what was previously predicted [19] and experimentally realized [20] in a nonsoliton form. In the second case, the system of GP equations for the matter-wave components, resonantly coupled by the magnetic component of the MW (microwave) field, admits an exact transition to the accelerating references frame, thus predicting stable 2D and 1D SA solitons, including VRs [33].

A challenging issue is a possibility of experimental realization of the predicted SA states. The theory also has a potential for development. In particular, as concerns the SA pairs of solitons with positive and negative masses, it is relevant to extend the analysis for the 2D system.

**Acknowledgments** – I thank Prof. Xiaojie Chen, EPL Deputy Editor, for the invitation to write a *perspective* article. This work was supported, in part, by the Israel Science Foundation through grant No. 1286/17.

- 
- [1] Gagnon L. and Belanger P. A., *Opt. Lett.* **15** (1990) 466-468.
  - [2] Parker D. F., Sophocleous C. and Radha C., *J. Phys. A: Math. Gen.* **35** (2002) 1283.
  - [3] Berry M. V. and Balazs N. L., *Am. J. Phys.* **47** (1979) 264-267.
  - [4] Siviloglou G. A. and Christodoulides D. N., *Opt. Lett.* **32** (2007) 979-981.
  - [5] Siviloglou G. A. *et al.*, *Phys. Rev. Lett.* **99** (2007) 213901.
  - [6] Voloch-Bloch N. *et al.*, *Nature* **494** (2013) 331-335.
  - [7] Minovich A. E. *et al.*, *Laser & Photonics Reviews* **8** (2013) 221-232.
  - [8] Efremidis N. K., Paltoglou V. and von Klitzing W., *Phys. Rev. A* **87** (2013) 043637.
  - [9] Zhang P. *et al.*, *Nature Commun.* **5** (2014) 4316.
  - [10] Clerici M. *et al.*, *Science Advances* **1** (2015) 1400111.
  - [11] Fu S. *et al.*, *Phys. Rev. Lett.* **115** (2015) 034501.
  - [12] Ellenbogen T. *et al.*, *Nature Phot.* **3** (2009) 395-398.
  - [13] Hu Y. *et al.*, *Opt. Lett.* **35**, 3952-3954 (2010).
  - [14] Jia S. *et al.*, *Phys. Rev. Lett.* **104**, 253904 (2010).
  - [15] Kaminer I., Segev M., and Christodoulides D. N., *Phys. Rev. Lett.* **106** (2011) 213903.
  - [16] Lotti A. *et al.*, *Phys. Rev. A* **84** (2011) 021807.
  - [17] Fattal Y., Rudnick A., and Marom D. M., *Opt. Exp.* **18** (2011) 17298-17307.
  - [18] Mayteevarunyoo T. and Malomed B. A., *Opt. Lett.* **40** (2015) 4947-4950.
  - [19] Batz S. and Peschel U., *Phys. Rev. Lett.* **110** (2013) 193901.
  - [20] Wimmer M. *et al.*, *Nature Phys.* **9** (2013) 780-784.
  - [21] Kivshar Yu. S. and Malomed B. A., *Rev. Mod. Phys.* **61** (1989) 763-915.
  - [22] Reyna A. S. and C. B. de Araújo, *Adv. Opt. Phot.* **9** (2017) 720-774.
  - [23] Abdullaev F. Kh. and Salerno M., *Phys. Rev. A* **72** (2005) 033617.
  - [24] Sulem C. and Sulem P.-L., *The Nonlinear Schrödinger Equation: Self-Focusing and Wave Collapse* (Springer, New York, 1999).
  - [25] Wang L., Malomed B. A. and Yan Z., *Phys. Rev. E* **99**, 052206 (2019).
  - [26] Sakaguchi H. and Malomed B. A., *Phys. Rev. E* **99** (2019) 022216.
  - [27] Chin C. *et al.*, *Rev. Mod. Phys.* **82** (2010) 1225.
  - [28] Pu H. *et al.*, *Phys. Rev. A* **67** (2003) 043605.
  - [29] H. Sakaguchi and Malomed B. A., *J. Phys. B* **37**, 1443-1459 (2004).
  - [30] Brazhnyi V. A. and Konotop V. V., *Mod. Phys. Lett. B* **18** (2004) 627.
  - [31] Malomed B. A., *Progr. Optics* **43** (2002) 71-193.
  - [32] Bludov Yu. V. and García-Ñustes M. A., *J. Phys. B: At. Mol. Opt. Phys.* **50** (2017) 135004.
  - [33] Qin J. *et al.*, *Phys. Rev. A* **99** (2019) 023610.
  - [34] Qin J., Dong G., and Malomed B. A., *Phys. Rev. A* **94** (2016) 053611.
  - [35] Sulem C. and Sulem P.-L., *The Nonlinear Schrödinger Equation: Self-Focusing and Wave Collapse* (Springer, New York, 1999).
  - [36] Fibich G., *The Nonlinear Schrödinger Equation: Singular Solutions and Optical Collapse* (Springer, Heidelberg, 2015).
  - [37] Kruglov V. I. *et al.*, *J. Phys. A: Math. Gen.* **21** (1988) 4381-4395.
  - [38] Quiroga-Teixeiro M. and Michinel H., *J. Opt. Soc. Am. B* **14** (1997) 2004-2009 (1997).
  - [39] Pego R. L. and Warchall H. A., *J. Nonlinear Sci.* **12** (2002) 347-394 (2002).
  - [40] Borovkova O. V. *et al.*, *Phys. Rev. E* **84** (2011) 035602(R).
  - [41] Driben R. *et al.*, *Phys. Rev. Lett.* **112** (2014) 020404.
  - [42] Sudharsan J. B. *et al.*, *Phys. Rev. A* **92** (2015) 053601.
  - [43] Reyna A. S. *et al.*, *Phys. Rev. A* **93** (2016) 013840.
  - [44] Zhang H. *et al.*, *Opt. Lett.* **44** (2019) 3098-3101.
  - [45] Malomed B. A., *Multidimensional Solitons* (AIP Publishing, Melville, 2022).